

## MODELLING OF FLOW INSTABILITIES UNDER SUPERCRITICAL CONDITIONS

**K. H. Leung, S. E. Langton, D. W. Hummel, and D. R. Novog**  
McMaster University, Hamilton, Ontario, Canada

### Abstract

A code utilizing the SIMPLE algorithm and the IAPWS-97 IF water properties was developed to examine mass flow instabilities in a heated pipe under supercritical conditions. Horizontal and upwards vertical cases were studied with the inlet enthalpy set to various nondimensional sub-pseudocritical numbers, and in all cases examined either flow excursions or oscillatory instabilities in the mass flow rate were observed. The results obtained suggest that an overpressure of the node adjacent to the inlet is responsible for the flow excursion, and we demonstrate that a modified dimensionless Euler number may be used as a criterion marking the onset of this phenomena. Junction form loss k-factors applied at the inlet and outlet increase the sensitivity of the pressure distribution to changes in velocity, and it is postulated that this contributes to the cause of the oscillatory instability.

**Keywords:** thermalhydraulics, thermophysical properties, supercritical instabilities

### 1. Introduction

One of the proposed concepts of the Generation IV Forum (GIF) is the Super Critical Water Reactor (SCWR). The novelty of this design is the reliance of a water coolant at a pressure and temperature above the critical point in order to improve the overall thermodynamic efficiency of the plant. The use of water under these conditions is not a new concept itself as fossil plants have already been constructed to operate in the supercritical regime, however the use in conjunction with a nuclear reactor is unique. The major advantage of the SCWR design is its potential for significant improvements in thermal efficiency, and hence in the economic benefits of such a plant.

From a thermalhydraulics perspective, one of the challenges posed by such a design is the abrupt variation in the density of the fluid as it is heated near its pseudo-critical point. This point is illustrated in Figure 1, and defined by [1] as where the specific heat capacity reaches a maximum when enthalpy is varied under constant pressure. Mass flow instabilities have been predicted under certain conditions, and this phenomena is being studied with both Computational Fluid Dynamics (CFD) and system codes as part of an international benchmark [2].

One of the biggest challenges posed with studying these phenomena is that the tools – specifically the system codes typically used for reactor analysis often require extensive modification of the source code to function in the supercritical region. In this study, the flow instability benchmark is re-examined using a 1-dimensional homogeneous thermalhydraulic code developed specifically to overcome these particular challenges. The main advantages to this approach are in the simplicity of the formulation and coding which allow for a more thorough understanding as compared to large scale 2-fluid nuclear systems codes which are considerably more complex

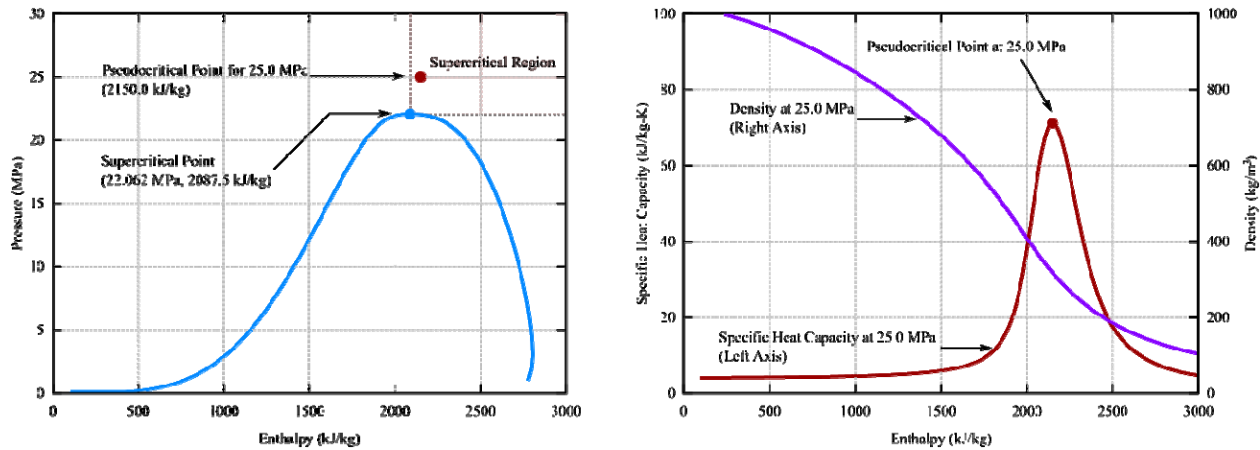


Figure 1 - Pseudocritical point of water at 25.0 MPa relative to the supercritical point (left); density and specific heat capacity at 25.0 MPa (right).

### 1.1. Benchmark overview

The geometry being examined by the benchmark consists of a single circular pipe with a length of 4.2672 m and an inner diameter of 8.36 mm. The inlet and outlet of the pipe are set at fixed pressures with k-factors applied to represent form losses. The working fluid is water, with an enthalpy which is fixed at the inlet. Heat is applied uniformly to the fluid along the length of the pipe and in the transient being investigated, it is increased linearly until a sharp fluctuation in the mass flow is observed. The effect of thermal capacity and conductivity of the tube materials were not included in the benchmark.

Two dimensionless numbers proposed by [1,2] are used to generalize the analysis. The sub-pseudocritical number defined in (1) is a measure of the magnitude with which the fluid at the inlet is below the pseudocritical point. A large value of  $N_{SPC}$  indicates that the fluid at the inlet has an enthalpy well below the pseudocritical point. The trans-pseudocritical number defined in (2) is a measure of the power to mass flow ratio at the onset of flow instability.

$$N_{SPC} = \frac{\beta_{pc}}{C_{p,pc}} (h_{pc} - h_{inlet}) \quad (1)$$

$$N_{TPC} = \frac{q}{\dot{m}} \frac{\beta_{pc}}{C_{p,pc}} \quad (2)$$

### 1.2. Code background

Modern nuclear thermalhydraulic codes are typically based on the Reynolds transport theorem which Ishii formalized to describe the transfer of mass, momentum and energy between two points in space and time [3]. Physical effects such as friction, junction losses or heat transfer are represented as source or sink terms in the respective equations. In the codes used for the analysis of Generation III and Generation III+ reactors, a separate set of equations are required for the vapour and liquid phases with jump conditions facilitating the interfacial transfer of properties.

Codes often rely on some form of implementation or approximation of the formulation defined by either the REFPROP package by the National Institute of Standards and Technology (NIST) or the International Association for the Properties of Water and Steam (IAPWS) to calculate the thermophysical properties of the fluid [4]. In the IAPWS-97 Industrial Formulation (IF), properties such as density, viscosity or specific heat capacity are determined from experiment and then fit as a function of pressure and either temperature or specific enthalpy or entropy.

Under the IAPWS-97 IF, the liquid and vapour phases of water are split into five regions of interest as illustrated in Figure 2 each with a separate set of equations defining the thermophysical properties [5]. In the figure, the supercritical region encompasses portions of regions 2, 3 and 5. Properties are available as a function of pressure and temperature or enthalpy for regions 1, 2, 3, and 4. Region 5 represents conditions where the fluid temperature is greater than 1073.15 K, and in this region, the IAPWS-97 IF does not contain equations to represent the properties as a function of pressure and enthalpy. The upper temperature bound of region 5 is 2073.15 K which is not illustrated in Figure 2.

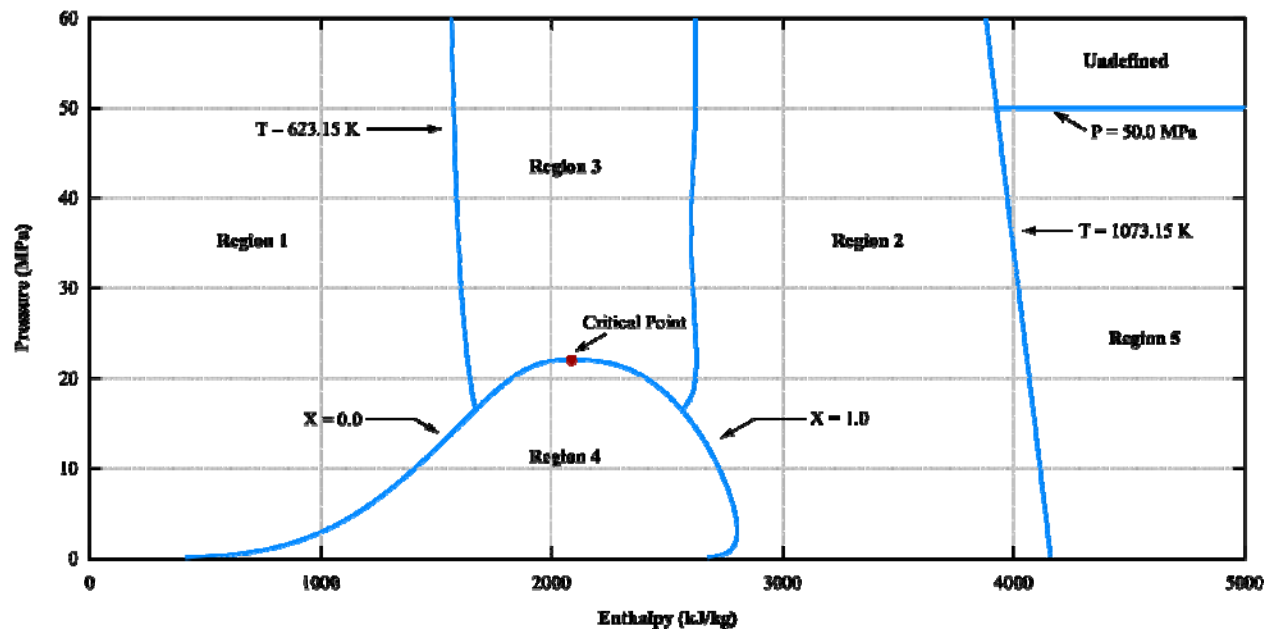


Figure 2 - IAPWS defined regions in terms of pressure and enthalpy

Although the nominal coolant operating conditions of proposed SCWRs is below the 1073.15 K threshold between Regions 2 and 5, the fluid temperatures very near the fuel clad and studies involving postulated accident scenarios will require codes to have access to water properties at these higher temperatures. Since some codes use enthalpy as the state variable it is important in the context of SCWR analysis to enable these codes to predict behaviour at these higher temperatures.

## 2. Method

### 2.1. Thermalhydraulic solver & nodalization

A one-dimensional thermalhydraulic solver was written in FORTRAN95 and solves Equations (3) – (5) using the Semi-Implicit Pressure Linked Equations (SIMPLE) algorithm on a staggered

grid [ 5 ]. These equations represent the conservation of mass, momentum and energy respectively. The terms on the right hand side of equation (4) represent the contributions to momentum from: pressure gradient, gravity, friction and form losses. Frictional losses are modelled using the Darcy-Weisbach friction factor which is approximated by the Swamee-Jain equation under turbulent conditions, and is assumed to be  $f = 64/Re$  for laminar flows. A Reynolds number of 2000 was used to approximate the boundary between laminar and turbulent flows. The correlation for the laminar flow regime is included for the purpose of completeness. In the scenarios being examined, the velocity at the inlet must approach the order of  $10^{-2}$  m/s before the transition between the two regimes occurs. In all of the cases examined, the only time this velocity is reached is well after the onset of flow instability. The source term in equation (5) indicates that the heat transfer is not explicitly computed, and instead, energy is directly added to the fluid. This assumption is deemed valid as the purpose of this study is to model flow instabilities, rather than heat transfer phenomena at the wall-fluid interface. The equations are deliberately kept simple in order to facilitate the study of the instability phenomena.

The code is configured to solve a single horizontal or vertical channel with pressure boundary conditions at the inlet and outlet. Pressure is solved at cell ‘nodes’, while velocity is computed at the cell faces as illustrated in Figure 3. When the density at a cell face is required, the average of the two surrounding nodes is used. The upwind approximation is used in modelling the advection of momentum and enthalpy.

$$\frac{\partial \rho}{\partial t} + \frac{\partial \rho u}{\partial x} = 0 \quad (3)$$

$$\frac{\partial \rho u}{\partial t} + \frac{\partial \rho u^2}{\partial x} = -\frac{\partial P}{\partial x} + \rho g + \frac{1}{2D_h} f \rho u^2 + \frac{1}{2} k \rho u^2 \quad (4)$$

$$\frac{\partial \rho h}{\partial t} + \frac{\partial \rho u h}{\partial x} = q''' \quad (5)$$

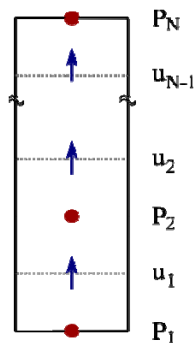


Figure 3 - Pressure-Velocity Grid Staggering

## 2.2. IAPWS-97 implementation

In order to find the thermophysical properties required, an implementation of the IAPWS-97 IF was created using FORTRAN95. Additional equations from the supplemental release for viscosity were added to the code to provide the additional properties required [6]. The entire implementation was verified against tabulated values provided in [4]. As noted previously, the major areas of interest are near the pseudo-critical point and in the region 2-5 boundary and hence particular attention is paid to the fluid properties in this domain.

### 2.3. Region 5 property fitting procedure

A region of interest is selected in terms of pressure and enthalpy, and an  $n \times m$  grid is created and illustrated in Figure 4. Since properties in region 5 are only available as a function of pressure and temperature, the function  $h(T, p)$  from the IAPWS-97 IF implementation was evaluated using a brute force method in order to determine a corresponding temperature for each grid point. With  $T(h, p)$  known at each point, the thermophysical properties can be evaluated using the IAPWS-97 IF implementation by evaluating  $f(T(h,p), p)$ .

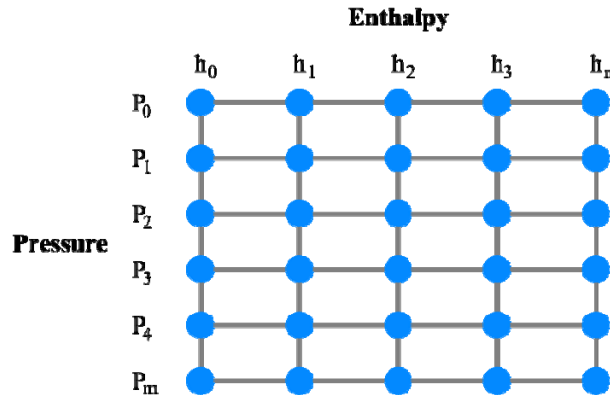


Figure 4 - Pressure-enthalpy grid

To fit the data points to polynomials, a script was created in MATLAB which uses the least squares interpolation method to define an  $N^{\text{th}}$  order polynomial over the pressure-enthalpy region of interest. Three dimensional least squares interpolation creates a polynomial of the following form:

$$f(h, p) = \sum_{i=0}^N \sum_{j=0}^N a_{ij} h^i p^j \quad (6)$$

In the equation,  $N$  is the order of the polynomial,  $a_{ij}$  are the polynomial coefficients,  $h$  is the enthalpy,  $p$  is the pressure, and  $f$  is the water property being fitted. The sum-squared error between the fitted polynomial and the values obtained from the IAPWS-97 IF implementation is defined as:

$$S = \sum_{d=1}^n \sum_{c=1}^m (f(h_d, p_c) - F(h_d, p_c))^2 \quad (7)$$

Where  $n$  and  $m$  are the number of grid points in enthalpy and pressure respectively, and  $F$  is the property as evaluated from the IAPWS-97 IF implementation. The goal is find a set of values for  $a_{ij}$  which minimizes  $S$ , therefore, the derivative of  $S$  with respect to  $a_{ij}$  is taken as:

$$\frac{\partial S}{\partial a_{ij}} = 2 \sum_{b=0}^N \sum_{c=0}^N \sum_{d=1}^n \sum_{e=1}^m (f(h_d, p_e) - F(h_d, p_e)) h_d^b p_e^c = 0 \quad (8)$$

Substituting equation (6) into equation (8) and rearranging yields:

$$\sum_{b=0}^N \sum_{c=0}^N \sum_{d=1}^n \sum_{e=1}^m \sum_{i=0}^N \sum_{j=0}^N a_{ij} h_d^i p_e^j h_d^b p_e^c = \sum_{b=0}^N \sum_{c=0}^N \sum_{d=1}^n \sum_{e=1}^m (F(h_d, p_e) h_d^b p_e^c) \quad (9)$$

The right hand side of (9) contains known terms from the IAPWS formulation and the pressure and enthalpy grid. On the left hand side of (9) the only unknown values are the coefficients  $a_{ij}$ . This equation is equivalent to the matrix equation  $Ax=B$  where  $x$  is an unknown value and  $A$  and  $B$  are matrices. Based on this, a MATLAB script was written to solve for the coefficients  $a_{ij}$ .

As an example, fit parameters are generated and provided Table 1 for density as a function of pressure and enthalpy and are used in conjunction with (10) for a third order polynomial. In the equation, the pressure is expressed as MPa and enthalpy as kJ/kg. The density returned is in units of  $\text{kg/m}^3$ .

**Table 1 – Coefficients for density as a function of pressure and enthalpy. The values are valid over the range  $23 \text{ MPa} < P < 30 \text{ MPa}$  and  $3800 \text{ kJ/kg} < h < 5800 \text{ kJ/kg}$ .**

$n_k$	$I_k$	$J_k$	$n_k$	$I_k$	$J_k$
8.05966E+01	0	0	1.16511E-05	0	2
6.23117E+00	1	0	-2.35164E-07	1	2
4.48503E-01	2	0	6.29591E-08	2	2
-6.07061E-03	3	0	-8.61600E-10	3	2
-5.32089E-02	0	1	-8.47417E-10	0	3
-6.34254E-04	1	1	3.49446E-11	1	3
-2.91268E-04	2	1	-4.54162E-12	2	3
3.95407E-06	3	1	6.28696E-14	3	3

$$\rho = \sum_k n_k P^{I_k} h^{J_k} \quad (10)$$

#### 2.4. Density Polynomial Accuracy

The accuracy of equation (10) with Table 1 may be evaluated by comparing the values generated by the polynomial and that of an arbitrarily generated data set using the  $\rho(p,T(p,h))$  function from the IAPWS-97 implementation. Figure 5 illustrates such a comparison for values between  $23 \text{ MPa} < P < 30 \text{ MPa}$  and  $3800 \text{ kJ/kg} < h < 5800 \text{ kJ/kg}$ . In the accuracy assessment, data points between the two values were generated at 0.5 MPa and 4 kJ/kg intervals. Over the entire grid, the average difference between the two values was  $0.004 \text{ kg/m}^3$  ( $\sigma = 0.061$ ), which suggests that over the stated range, the polynomial provides an accurate representation of  $\rho(p,h)$ . Of additional interest is the derivative of the density with respect to enthalpy. Using the same method, the average difference between the two values was  $(-4.74)(10^{-5}) \text{ kg/m}^3 / \text{kJ/kg}$  ( $\sigma = 0.0007$ ), and the same conclusion as before may be drawn.

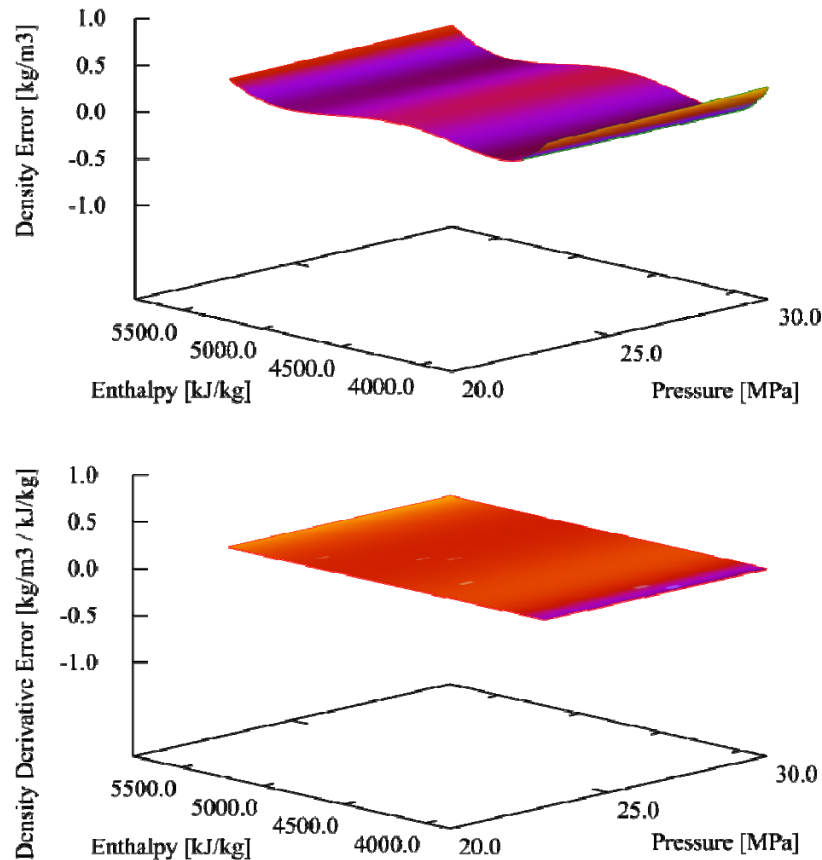


Figure 5 - The absolute accuracy of the polynomial for  $\rho(P,h)$  (top) and  $d\rho/dh$  (bottom) as computed using

### 3. Results

#### 3.1. Comparison of the HEM code vs. CFD

STAR CCM+, a commercially available CFD code, was used to verify the predictions made by the in-house code. For the comparison, the geometry being studied in the benchmark is modelled using a mesh consisting of approximately 2 million faces, and this is illustrated in Figure 6.

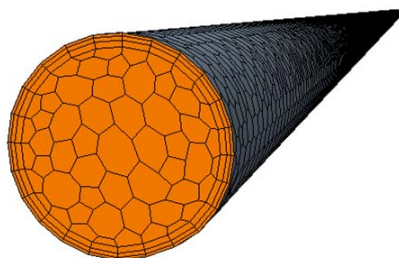


Figure 6 - STAR CCM+ mesh of benchmark geometry

The STAR CCM+ simulations were performed using the segregated enthalpy solver. This executes calculations using enthalpy as the independent variable. The water properties used in

the simulation were integrated into the program using polynomial fits over the required enthalpy-pressure range. The polynomials were created in the same manner as for the Region 5 property fits described in Section 2.3. Turbulence was modelled using the standard  $k-\epsilon$  model and the High  $y^+$  Wall Treatment. In addition, the Standard Wall Function was used.

A reference case was run with both the in-house and CFD codes using the conditions specified in Figure 7. The inlet mass flows for both the in-house code and CFD code are compared in Figure 7, and qualitatively, the mass flow rates predicted by both codes follow very similar trends, with the CFD code predicting a slightly higher mass flow rate, although this is to be expected. From this, we conclude that the in-house code produces reasonable results for the transients being examined.

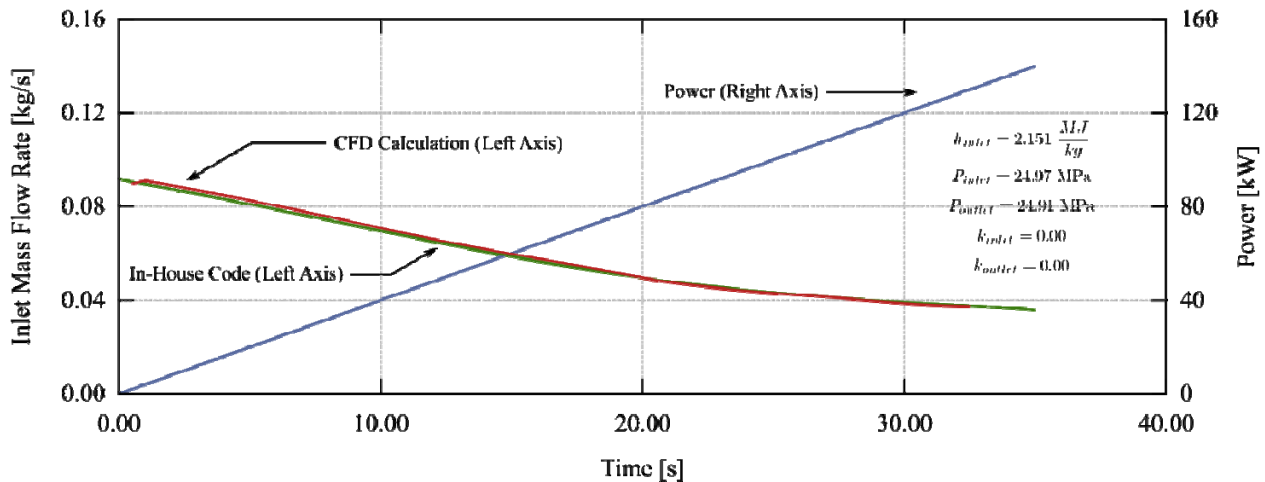


Figure 7 - Inlet mass flow rate comparison between the in-house code and STAR CCM+ for a rapid power increase under supercritical conditions.

### 3.2 Transient Classifications

In the transients being examined, the pressure at the inlet and outlet are fixed at 25.0 and 24.9 MPa respectively. The power applied to the pipe is increased with time, causing the mass flow rate to decrease in the transient until one of three things occur:

1. An excursionary or ‘Ledinegg’ instability occurs when the pressure demanded by the system at a given mass flow exceeds that which is available [7]. In boiling flows, this leads causes the mass flow rate to ‘jump’ to a different value. For the purposes of this study, we stipulate that in a Ledinegg instability, the mass flow must be driven to a non-zero value. These instabilities were not conclusively observed in the current study, although [8] has postulated that for the geometry being examined, they exist under conditions with high degrees of inlet subcooling. A candidate case is presented in Figure 8 where a Ledinegg instability may be present, but is masked by mass flow oscillations. The highly subcooled inlet ( $N_{SPC} = 3.00$ ) and characteristic sudden reduction of the mass flow to a non-zero value support this assertion, albeit not conclusively.
2. Inlet overpressure is similar in nature to the Ledinegg instability in that the system demands more pressure than is available, however a second non-zero mass flow solution to the momentum equation does not exist. In this case, the mass flow is driven to the

trivial solution, and this was commonly observed in cases where the inlet enthalpy was close to the pseudo-critical point. This type of transient scenario is characterized by a rapid increase in the trans-pseudocritical number, and an example case where this is observed is illustrated in Figure 9.

3. Oscillatory instabilities occur when the fluid in the pipe reaches a state where more than one mass flow rate solution occurs for a given pressure. Given the transient nature of the system, these instabilities are characterized by a periodic variation in the mass flow rate with respect to time. The majority of the instabilities observed in the cases examined were of this type, and an example of a transient yielding one is illustrated in Figure 10.

Although the above scenarios are clearly observed qualitatively in the example plots, both the Ledinegg or inlet overpressure cases are characterized by sharp changes in the mass flow rate when crossing the stability threshold. Since the trans-pseudocritical number is a function of the power to mass flow ratio, this value also changes rapidly in the region of interest. In order to create a consistent stability map, numerical criteria are required to ascertain the threshold where the flow becomes unstable.

For a pipe with fixed pressures at both the inlet and the outlet, if the power increases over the course of the transient, both the average density and the mass flow in the pipe are expected to monotonically decrease. For this analysis, the criterion used to define the onset of the oscillatory instability is the point where the derivative of mass flow rate with respect to time is positive (11). In order to remove scenarios where this criteria is fulfilled spuriously due to the solver adjusting the time-step size to match the Courant limit, the reported results represent 5 consecutive time-steps which fulfil this condition.

$$\frac{d\dot{m}}{dt} > 0 \quad (11)$$

Detecting the onset of the Ledinegg instability or the overpressure scenario is more complicated since the sign of the mass flow time derivative stays the same throughout the transient. The authors in [9] calculated the time derivative of the trans-pseudocritical number at each point in the transient, and considered the flow to be unstable when (12) was fulfilled.

$$\frac{dN_{TPC}}{dt} > 0.1 \quad (12)$$

In the current study we have found that the choice of the rate of power increase affects when this condition is fulfilled. Instead, we propose a modified form of the Euler number be used (13). In this equation the pressure differential refers to the pressure drop across the first two nodes of the test section, while the terms in the denominator represent the contributions due to gravity, friction and junction form losses.

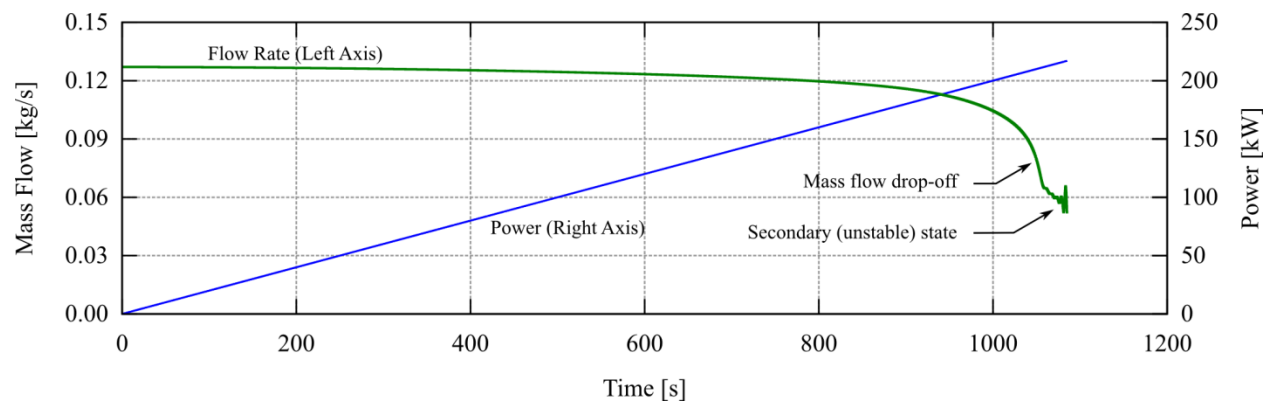
$$Eu^* = \frac{P_{IN} - P_2}{\rho g \Delta z + \left( \frac{f}{2D_h} + \frac{k}{2} \right) \rho u^2} \quad (13)$$

The basis of the use of this criteria stems from the conservation of momentum equation, (4). Since we are using an upwind approximation in our solution approach, the mass flux in the first cell has no dependence on the  $d\rho u^2/dx$  term, therefore the sum of the sources and sinks becomes equal to the mass flux time derivative term. For most of the transient, the ratio of the momentum sources to the sinks is slightly under 1.0 since our mass flux is gradually decreasing with time. If the solution gets to a point where the driving pressure at the inlet node is insufficient to overcome the losses, there is a very rapid drop in this ratio which is illustrated in Figure 9b. For this study, we consider (14) to be the condition which marks the onset of an overpressure scenario, and monitor for points in the transient where either (12) or (14) are met.

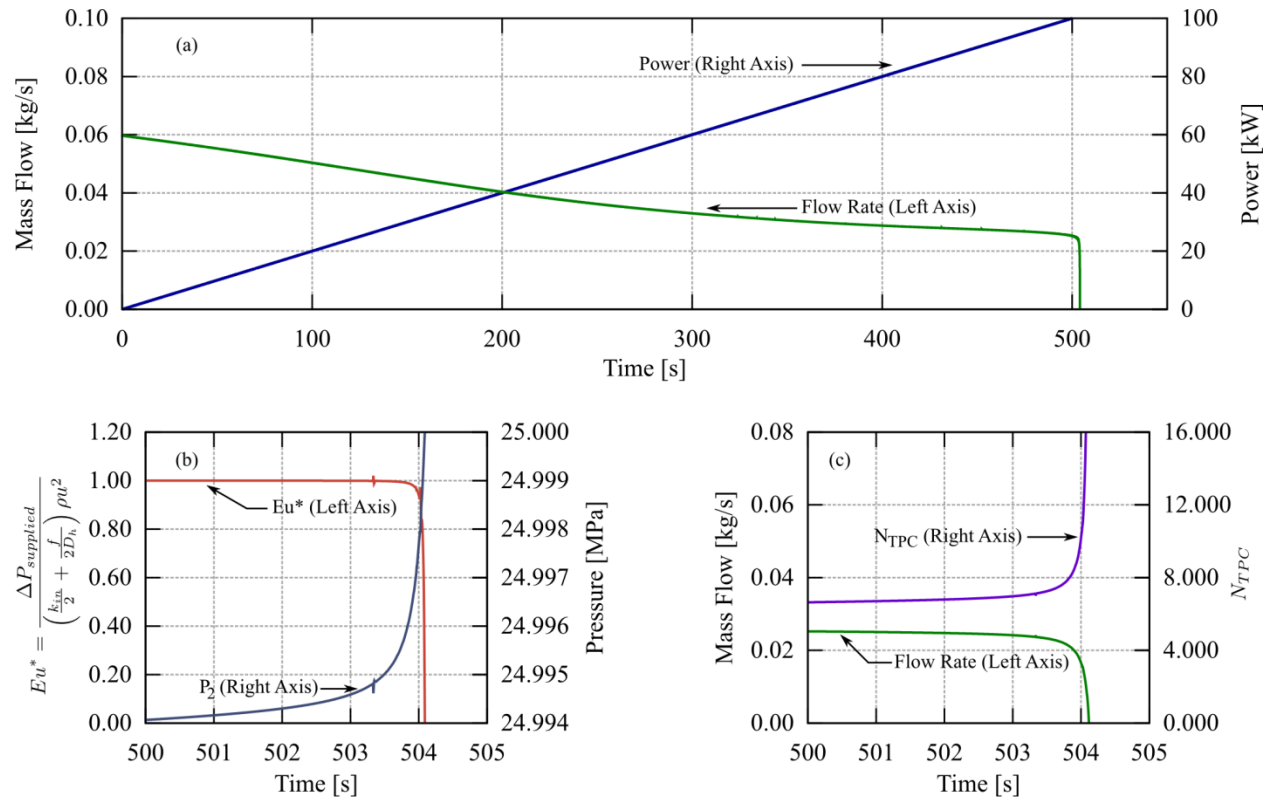
$$Eu^* < 0.9995 \tag{14}$$

Figure 11 illustrates how the onset of flow instability in an oscillatory transient has a dependence on the number of nodes used. The  $N_{TPC}$  value reported decreases as more nodes are added, which is in general agreement with the trends observed by [10]. For the purposes of this study, 25 nodes were used, which as the figure suggests may tend to produce higher values of  $N_{TPC}$  at the onset of instability. The implication of this is that the initiating conditions of the instability may be suppressed by averaging the fluid properties over a larger cell.

For the transients reaching higher values of  $N_{TPC}$  – specifically those at low inlet subcooling and small outlet k-factors – the enthalpy of the fluid exceeds the range of the defined interpolated polynomial. While the general trends of the fluid properties are preserved (density decreases with increasing enthalpy for example), the error in the density exceeds 5% at  $h > 6300$  kJ/kg at 25 MPa.



**Figure 8 - Example case (Horizontal,  $N_{SPC} = 3.00$ ,  $K_{OUT} = 2$ ) illustrating the progression of a transient until the occurrence of a flow instability.**



**Figure 9 - Sample case (Horizontal,  $N_{SPC} = 0.00$ ,  $K_{OUT} = 20.0$ ) where a rise in inlet pressure causes mass flow to drop to zero. (a) Power and mass flow rate through the course of the transient. (b) Modified Euler number and pressure in the node immediately adjacent to the inlet in the final 5 seconds of the transient. (c) Mass flow rate and  $N_{TPC}$  in the final 5 seconds of the transient.**

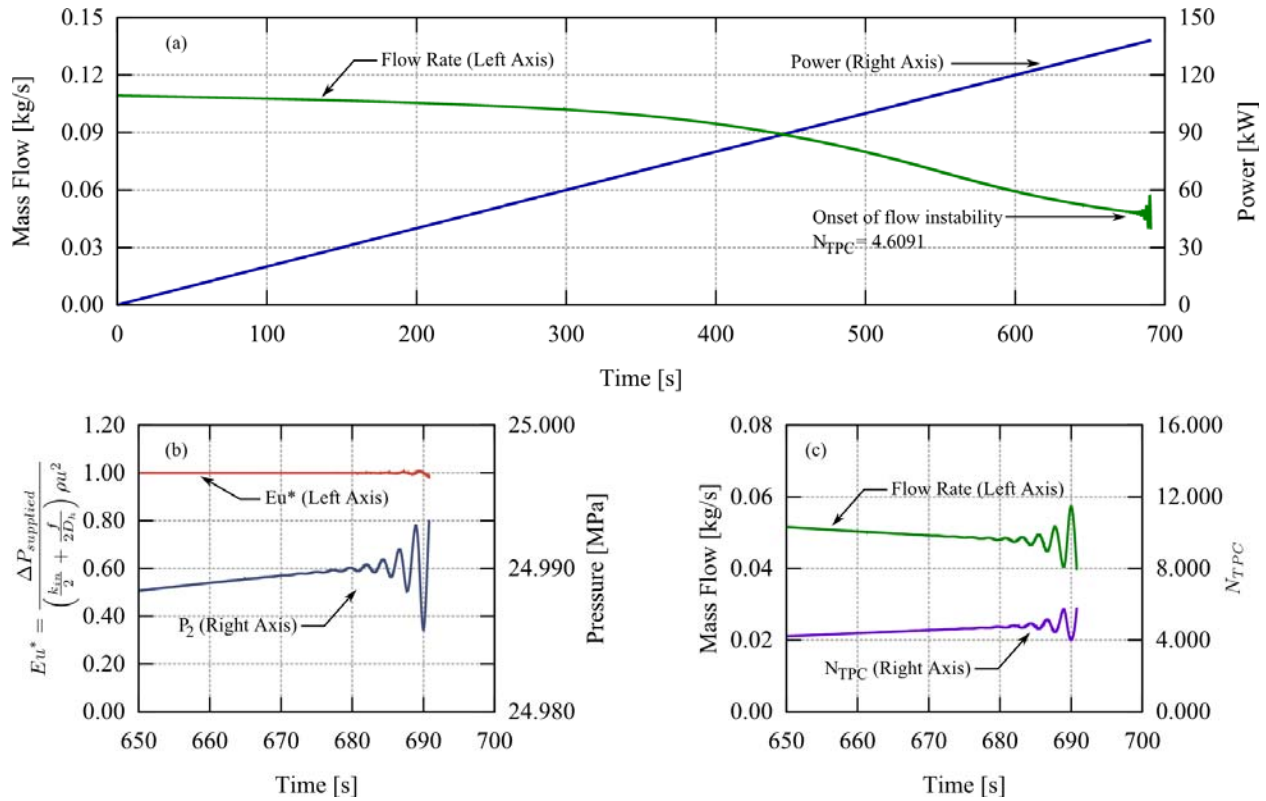


Figure 10 - Sample case (Horizontal,  $N_{SPC} = 1.50$ ,  $K_{OUT} = 5$ ) illustrating the progression of a transient until the occurrence of an oscillatory flow instability. (a) Power and mass flow rate through the course of the transient. (b) Modified Euler number and pressure in the node immediately adjacent to the inlet in the final 50 seconds of the transient. (c) Mass flow rate and  $N_{TPC}$  in the final 50 seconds of the transient.

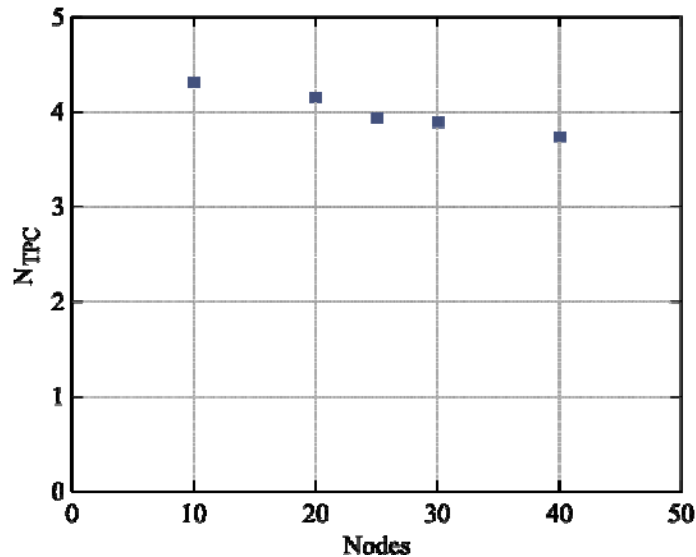


Figure 11 - Dependence of the  $N_{TPC}$  at the onset of flow instability on the nodalization scheme. A single case (Horizontal,  $N_{SPC} = 1.00$ ,  $K_{OUT} = 10$ ) is run using nodalization schemes containing between 10 and 40 nodes. In all of the cases illustrated in the figure, oscillatory behaviour was observed. In all other cases, 25 nodes were used.

### 3.3. Instability Maps

Both horizontal and vertical cases were run using different values for the outlet form loss coefficient and inlet enthalpy. The preliminary horizontal and vertical instability maps are illustrated in Figure 12 and Figure 13 respectively. The trans-pseudocritical number corresponding to when the instability criteria is fulfilled is reported for each case run, and with the exception of the indicated cases, all instabilities were oscillatory in nature.

On a qualitative basis, the trends illustrated in the current stability maps are similar to those created using linear stability codes by [11].

- Both the current study and [11] predict that for a given outlet junction loss factor, the flow is least stable when the inlet subcooling number is around  $N_{SPC} = 1.0$ .
- In terms of the dimensionless parameters, very little difference was observed between the horizontal and vertical maps. The only noticeable difference was that the vertical cases seemed more prone to undergoing oscillatory instabilities at high subcooling and high outlet loss factors.
- No oscillations were observed at  $N_{SPC} = 0.0$ , however addition cases should be run with a higher pressure differential to verify the stability at this inlet enthalpy.
- An increase in the outlet k-factor reduces the  $N_{TPC}$  at which the flow becomes unstable, suggesting that the flow is less stable with higher junction loss coefficients.
- The transients marked ‘non-oscillatory transients’ are characterized by a reduction in the mass flow to zero at the points indicated. The sample transient in Figure 9 represents what is typically observed in these cases.

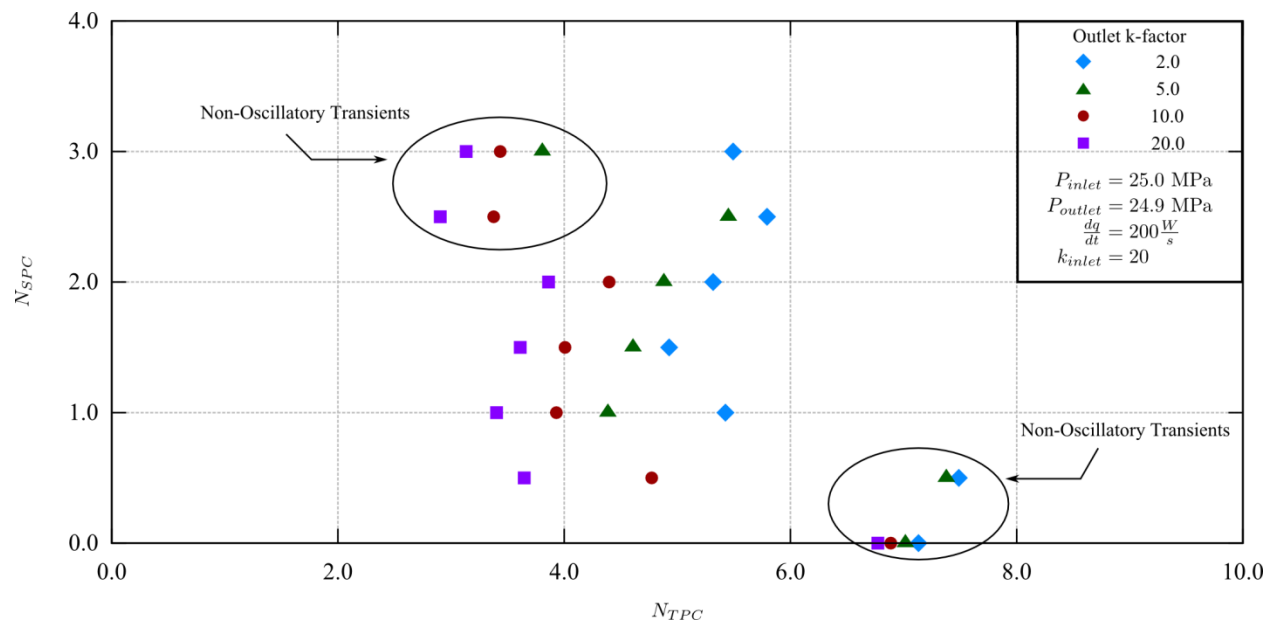


Figure 12 - Horizontal flow stability map illustrating  $N_{SPC}$  and  $N_{TPC}$  where the criteria for flow instability was met.

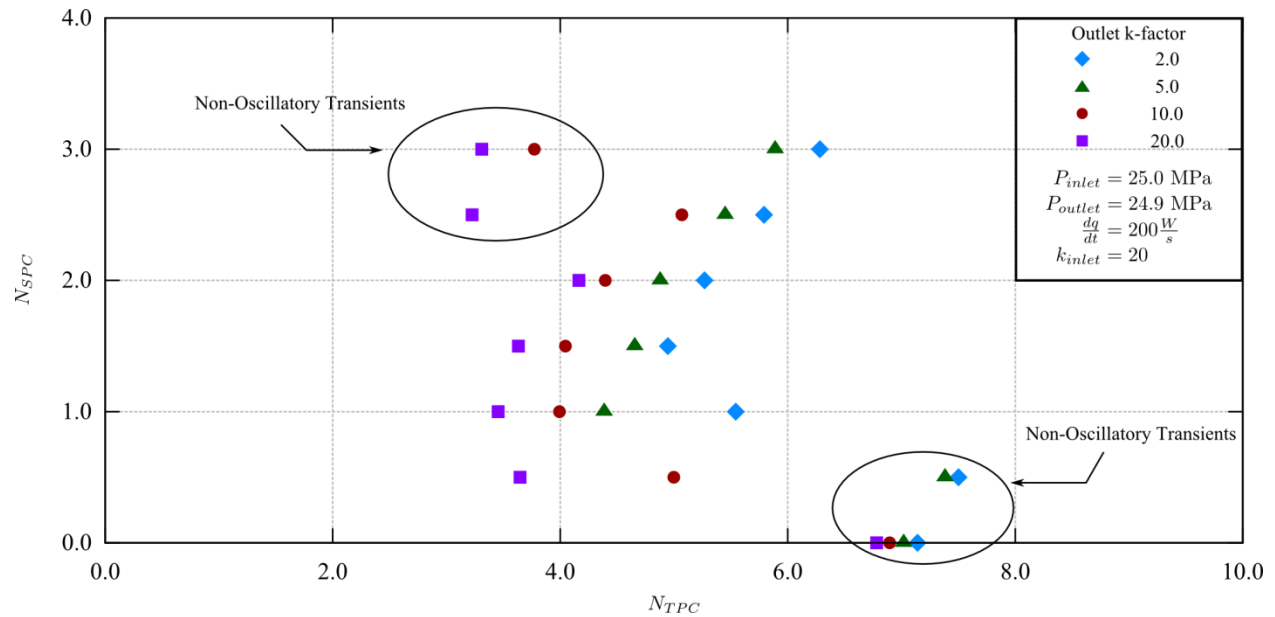


Figure 13 - Vertical flow stability map illustrating  $N_{SPC}$  and  $N_{TPC}$  where the criteria for flow instability was met.

#### 4. Conclusions

A transient HEM thermohydraulic solver and water property package were developed to model the stability of flows under supercritical conditions. In doing this, a set of equations mapping the thermophysical properties of water as function of pressure and enthalpy were generated for the region  $T > 1073.15$  K. The solutions being returned by the code were confirmed against a CFD simulation and deemed to be of a reasonable nature. The code is now available for performing steady state and transient simulations of transitional SCWR flows under different operating conditions.

In the course of mapping the stability threshold, oscillatory instabilities were most commonly observed, although in multiple cases the mass flow was driven abruptly to zero. It was postulated that this was caused by the pressure in the node adjacent to the inlet rising to the point where the differential pressure was insufficient to overcome the losses from gravity, the k-factor and friction. To this end, a modified Euler number was used to monitor for the point where this occurred. The existence of Ledinegg instabilities was not definitively confirmed, although there are cases in the high subcooling region where this is suspected.

#### 5. References

- [1] W. Ambrosini, On the analogies in the dynamic behaviour of heated channels with boiling and supercritical fluids, *Nuc. Eng. Des.*, 237, pp. 1164-1174, 2007.
- [2] W. Ambrosini, Specifications for a benchmark exercise on flow stability in heated channels with supercritical fluids, University of Pisa, Italy, 2009.

- [3] M. Ishii and T. Hibiki, Thermo-Fluid Dynamics of Two-Phase Flow, Springer Science, New York, USA, 2006.
- [4] W. Wagner and H. J. Kretzschmar, International Steam Tables Properties of Water and Steam Based on the Industrial Formulation IAPWS-IF97, Springer Berlin Heidelberg, 2008.
- [5] S. V. Patankar, Numerical Heat Transfer and Fluid Flow, Hemisphere Publishing, 1980.
- [6] International Association for the Properties of Water and Steam, *Release on the IAPWS Formulation 2008 for the Viscosity of Ordinary Water Substance*, available at <http://www.iapws.org> (September 2008).
- [7] R. T. Lahey, Jr. and F. J. Moody, The Thermal-Hydraulics of a Boiling Water Nuclear Reactor, 2nd ed., La Grange Park : American Nuclear Society, 1993.
- [8] W. Ambrosini and M. Sharabi, Dimensionless parameters in stability analysis of heated channels with fluids at supercritical pressure, *Nuc. Eng. Des.*, 238, pp. 1917-1929, 2008.
- [9] F. Fiori, RELAP5/Mod3.3 and TRACE5.0 predictions of heat transfer and stability for supercritical water flow in heated pipe, presented at the IAEA Technical Meeting on Heat transfer, thermal-hydraulics and system design for supercritical pressure water cooled reactors, Pisa, Italy, 2010.
- [10] W. Ambrosini, Assessment of flow stability boundaries in a heated channel with different fluids at supercritical pressure, *Ann. Nucl Energy*, in press (2010).
- [11] W. Ambrosini, Discussion on the stability of heated channels with different fluids at supercritical pressures, *Nuc. Eng. Des.*, 239, pp. 2952-2963, 2009.